第33卷 第8期 焊 接 学 报 Vol. 33 No. 8
2012年8月 TRANSACTIONS OF THE CHINA WELDING INSTITUTION August 2012

不锈钢低真空加热过程去膜机理分析

何 鹏[1]， 郑岩松[1]， 李 军[1,2]， 钱乙余[1]， 娄豪月[2]， 张文锋[2]

(1. 哈尔滨工业大学 先进焊接与连接国家重点实验室，哈尔滨 150001；
2. 浙江银轮机械股份有限公司，台州 317200)

何 鹏

摘 要： 在低真空条件下对供应态及800 ℃空气中氧化过的0Cr18Ni9不锈钢进行加热，同时对供应态不锈钢板进行熔融铜中浸泡试验. 结果表明，低真空加热使不锈钢表面氧化膜结构发生变化，而这种氧化膜不能阻止熔融铜对不锈钢板的大量溶解. 通过对真空钎焊不锈钢去膜机理的探讨以及热力学计算，提出低真空条件下碳能够起到还原松动氧化膜的作用；当熔融铜沿着开裂的氧化膜流动接触到不锈钢基体，在Ni原子向液态铜中优先扩散的带动下，不锈钢快速溶解并将氧化膜抬起，在表面张力作用下最终实现低真空钎焊氧化膜的彻底破除.

关键词： 不锈钢低真空钎焊；去膜机理；碳还原作用；氧化膜；溶解

中图分类号： TG454 **文献标识码：** A **文章编号：** 0253－360X(2012)08－0093－04

0 序 言

采用镍基、铜基钎料在高温高真空条件下通常能够实现不锈钢的高质量钎焊，国内外学者认为得到高质量钎焊接头的前提是高真空条件下实现了不锈钢表面氧化膜的去除[1-3]. 但对于高真空条件下不锈钢的去膜机理，尽管国内外学者进行了大量的研究，但至今仍存在多种不同观点，具体去膜过程仍不是很清楚.

不锈钢除含主要元素Fe和C外，往往还含Cr，Ni，Mn，Ti，Mo，Nb等合金元素. 在不锈钢表面形成的氧化物中，Cr_2O_3和TiO_2相当稳定，比较难去除[1,4]. 对于高真空不锈钢表面的去膜机理，文献[2]指出，在1.0×10^{-3} Pa真空度下，不锈钢表面的Cr_2O_3在1 000 ℃时能够直接挥发去除；而另有研究表明碳是真空钎焊时不锈钢表面氧化膜还原的主要因素[5]. 对于1Cr18Ni9Nb不锈钢来说，在1.0×10^{-3} Pa真空度下，当加热温度达到900 ℃，只要少量的碳就能还原其表面的氧化膜，当不锈钢表面氧化膜开裂时，钎料即能渗过开裂的氧化膜润湿母材[3].

在低真空加热时不锈钢去膜机理方面的研究非常有限，也未形成相关理论. 文中通过试验研究和理论分析，对低真空加热不锈钢的去膜机理进行探索，为实际生产中确定低真空产品可钎焊性及制定合理钎焊工艺奠定基础.

1 试验方法

试验以0Cr18Ni9不锈钢和纯铜钎料为研究对象，将供应态不锈钢板以及800 ℃空气中氧化过的不锈钢板在ZJYL-160型石墨加热真空炉中按图1所示工艺曲线加热，炉温接近1 000 ℃时，真空度达到最高并维持在0.1 Pa左右，并在相同条件下完成纯铜钎料在两种状态不锈钢板上的铺展试验. 对两种不锈钢板加热前后表面宏观、微观形貌变化及钎料铺展情况进行对比分析.

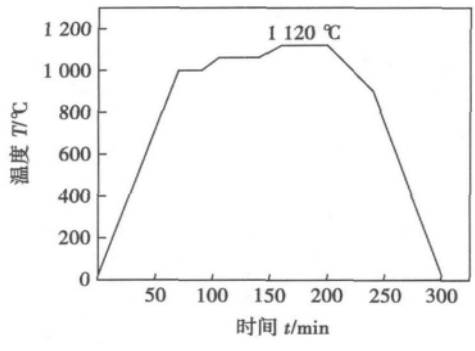

图1 不锈钢真空钎焊工艺曲线

Fig. 1 Temperature curve of stainless steel vacuum brazing

收稿日期：2011－05－16

以陶瓷坩埚为熔融铜的容器对厚度为 300 μm 的 0Cr18Ni9 不锈钢按图 1 所示真空加热曲线进行浸泡试验. 对低真空加热后的试样沿着垂直于不锈钢板的平面进行解剖、研磨、抛光,用质量分数 6% 的硫酸铜盐酸溶液浸蚀,并用光学显微镜、扫描电镜(SEM)观察不锈钢与铜界面附近微观组织,用能谱仪(EDS)对不锈钢与铜的溶解扩散情况进行定量分析.

2 试验结果与讨论

2.1 低真空加热不锈钢表面结构变化

对供应态及 800 ℃空气中氧化过的 0Cr18Ni9 不锈钢在低真空下加热,图 2 为供应态不锈钢加热前后表面形貌,图 3 为 800 ℃空气中氧化过的不锈钢加热前后表面形貌. 供应态不锈钢板加热后表面发亮,而 800 ℃空气中氧化过的不锈钢板表面呈暗红色,低真空加热后氧化色褪去,而且表面重新变得光亮,光亮度与供应态不锈钢低真空加热后的相同;真空加热后两种不锈钢板表面呈现出相同的微观形貌,在未经金相腐蚀的情况下,可以在电镜下直接观察到晶界以及晶粒长大趋势;同时铺展试验发现,低真空加热条件下,纯铜钎料在供应态及空气中氧化过的不锈钢板上均发生良好润湿铺展,且钎料铺展面积相当.

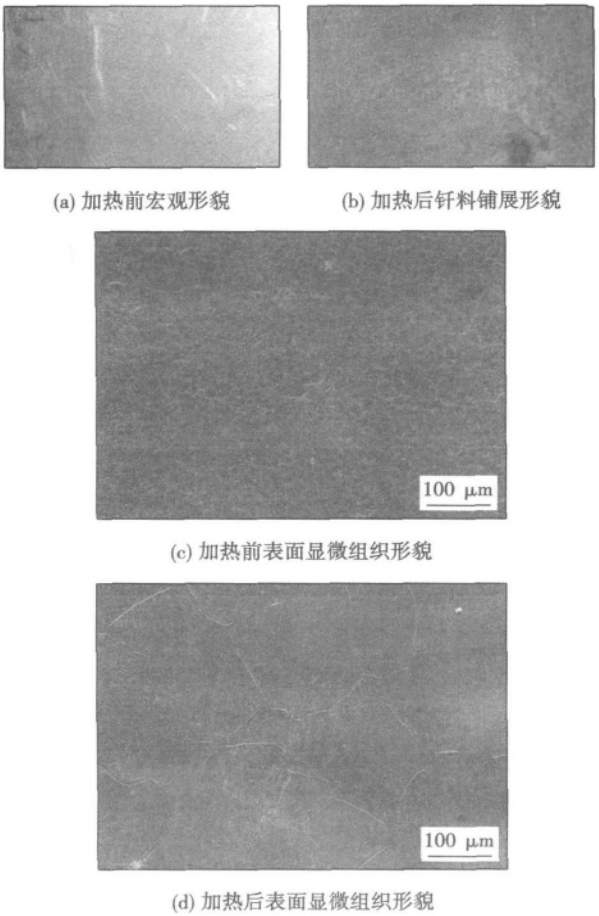

图 2 供应态不锈钢加热前后表面形貌

Fig. 2 Surface morphology of commercial stainless steel

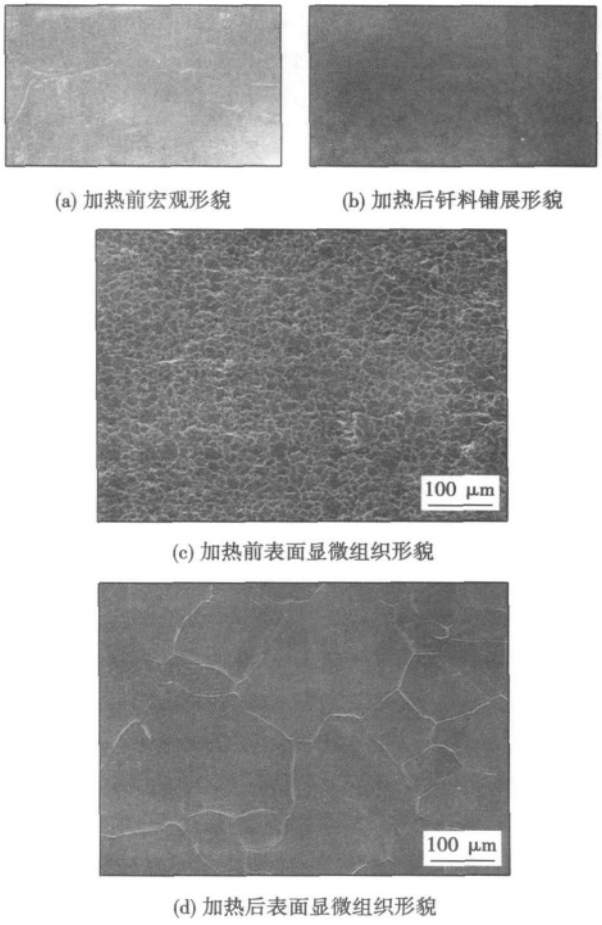

图 3 800 ℃空气中氧化过的不锈钢加热前后表面形貌

Fig. 3 Surface morphology of stainless steel oxidized at 800 ℃ in atmosphere

不锈钢板经 800 ℃空气中加热后,表面氧化程度加重,而且氧化变色表明氧化膜结构也发生了变化;低真空加热后不锈钢板表面的暗红氧化色褪去,表明预氧化结构变化的氧化膜已经消失. 而晶界的显现及钎料的铺展进一步证明低真空加热不锈钢表面氧化膜已经去除.

不锈钢在加热过程中 C 原子能够快速向不锈钢晶界迁移[6],且真空炉加热过程会出现石墨棒的烧损,C 原子挥发进入炉内空间. 这两种来源的 C 原子都将与不锈钢表面接触,因此真空条件下还原性很强的 C 原子可能与氧化膜发生反应. 文献[7]指出 1 000 ℃时 CO 分压只需低于 13 Pa 就能使 Cr_2O_3 被碳还原,发生如下反应,即

$$Cr_2O_3 + 3C \rightarrow Cr + 3CO \quad (1)$$

为了验证试验条件下碳对氧化膜作用的可能性,在 1 000 ℃,0.1 Pa 条件下利用热力学进行计算分析.

假定供应态不锈钢和经 800 ℃空气中氧化过的不锈钢表面氧化膜中的 $Cr_2O_3(x)$ 和 $Cr_2O_3(y)$ 均与碳发生如式(1)的氧化还原反应,则反应能否正向进行取决于吉布斯自由能变,即

$$\Delta_r G_m(T) = \Delta_r G_m^\theta(T) + RT\ln Q \quad (2)$$

式中: $\Delta_r G_m^\theta(T)$ 为标准摩尔生成吉布斯自由能; R 为气体常数; T 为温度; Q 为反应熵, $\Delta_r G_m^\theta(T)$ 和 Q 分别为

$$\Delta_r G_m^\theta(T) = \Delta_r H_m^\theta - T\Delta_r S_m^\theta \quad (3)$$

$$Q = \frac{[c(Cr)/c^\theta]^2 [p(CO)/p^\theta]^3}{[c(Cr_2O_3)/c^\theta] [p(C)/p^\theta]^3} \quad (4)$$

式中: $\Delta_r H_m^\theta$, $\Delta_r S_m^\theta$ 分别为反应摩尔焓变和摩尔熵变; c, p 分别为未达到平衡时任意态物质的浓度和分压; c^θ 为标准浓度; p^θ 为标准压力.

在 1 000 ℃,0.1 Pa 低真空条件下对式(1)进行热力学计算,可得

$$\Delta_r G_m(T) = -328.49 < 0 \quad (5)$$

说明 Cr_2O_3 可以被碳还原.

2.2　不锈钢与熔融铜界面作用对去膜的影响

低真空条件下将不锈钢浸泡在熔融铜中所发生的界面溶解扩散试验将有助于分析研究真空钎焊过程的去膜机理.

试验结果表明,1 120 ℃下不锈钢板与熔融铜在接触后发生强烈相互作用,浸泡后的不锈钢厚度从 300 μm 下降到 120 μm. 图 4 为铜在不锈钢中的晶间渗入形貌,图 5 为不锈钢晶粒上快速扩散溶解区的形貌. 从图 4 和图 5 中可以看到,该溶解过程不是整齐划一地进行的,界面处表现出显著的优先溶解,不锈钢表面出现明显下凹. 利用能谱仪进行分析,测试结果见表 1. 可见晶粒边缘及晶粒局部率先出现的发黑区域铬、镍含量显著下降,而铜含量较高,均超过铜在奥氏体不锈钢中的极限固溶度 7.3%. 根据试验现象和文献[8]可以判定,晶粒上的发黑现象是 Cu 原子向不锈钢中扩散超过极限固溶度引发相变造成的.

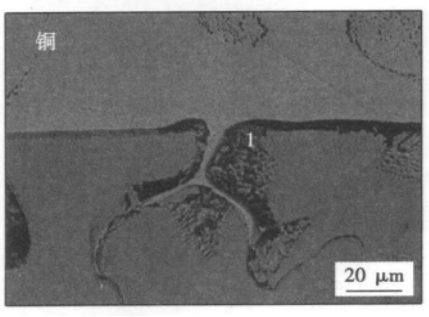

图 4　铜在不锈钢中的晶间渗入形貌

Fig. 4　Microstructure of intergranular penetration of stainless steel

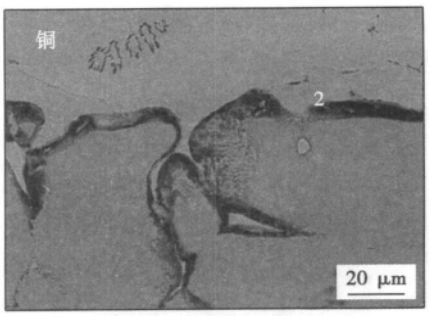

图 5　不锈钢晶粒上快速扩散溶解区形貌

Fig. 5　Microstructure of rapid diffusion and solution zone of stainless steel

表 1　不锈钢晶粒上相变区域成分(质量分数,%)

Table 1　Chemical compositions of specified area

位置	C	Cr	Fe	Ni	Cu
1	1.29	16.16	69.77	1.96	7.32
2	1.63	17.68	68.16	2.58	9.58

0Cr18Ni9 不锈钢易出现宏观晶间渗入现象,是因为晶界处存在大量的晶体缺陷. 当液态铜与不锈钢表面接触时迅速向不锈钢内扩散,并在晶界处聚集形成微小液膜,此时两侧的晶粒与液态铜接触,不锈钢的基体原子随之开始向该液膜中扩散溶解. 而且由于镍与铜物理性能接近,二者固液态下均能无限互溶,使不锈钢晶粒表面的 Ni 原子极易迁移进入液态铜膜. 在试验中也看到,在晶粒发黑的边缘 Ni 原子含量有显著的下降,Ni 原子的迁移还破坏附近区域晶格结构,提高了该区域能量,带动不锈钢基体其它原子也易于向液态铜中迁移,并在浓度梯度作用下向晶界外运动,同时 Cu 原子也易于向该区域迁移扩散进入不锈钢基体,铜大量富集超过不锈钢中的极限固溶度时使晶粒边缘相变发黑. 这种相互作用持续进行,晶界铜液膜不断拓宽便形成宏观晶间渗入.

当这种晶间渗入逐渐扩展包围了整个晶粒,晶粒便脱离母材基体,整个晶粒表面同时与液态铜接触,加速了二者的相互作用,该晶粒将很快由于铜的大量扩散出现相变,呈黑色颗粒悬浮在母材基体附近,随着时间延长逐渐完全溶解到液态铜中.

不锈钢薄板经轧制成形过程中的强烈变形使位错密度急剧增加 5 ~ 6 个数量级,并交织形成位错

网,位错网密集区成为不锈钢基体原子向外运动的方便通道,Ni 原子优先沿着位错网向外扩散,并带动其它原子向液态铜中迁移,因此不锈钢表面各处溶解速度的差异使其形成了凹凸不平的状态.

2.3 不锈钢低真空钎焊去膜机理分析

不锈钢板低真空加热后的表面已经完全失去原始形貌,而且某些区域氧化膜的变化更为突出,使不锈钢表面形成相互交汇的沟槽,并将表面分割成大块区域. 而且根据前面的分析可知,表面氧化膜的变化主要来自内部碳的还原反应,这个反应发生在不锈钢基体与氧化膜的界面上,势必导致氧化膜的松动. 被还原弱化的氧化膜发生松动后,由于不锈钢基体与氧化膜膨胀系数存在差异,加热过程中产生的形变应力将使氧化膜发生破裂.

在不锈钢与熔融铜接触前,由于空间仍有氧分压的存在,当不锈钢表面氧化膜产生裂缝后,还会在氧的作用下再形成新的氧化膜,不锈钢表面氧化膜此时处在动态变化的过程中. 当液态铜遇到这样的不锈钢表面就会在裂缝毛细作用下快速流动并与不锈钢基体相接触. 根据不锈钢与液态铜相互作用特点可以发现,即使少量液态铜与不锈钢板接触,在 Ni 原子带动下不锈钢基体原子也会快速溶解. 不锈钢基体的溶解将促使 Cu 原子不断向该部位聚集,这个过程持续进行,类似晶间渗入形成的过程,逐渐在基体晶粒表面与氧化膜间形成铜液膜,氧化膜漂浮在液态铜上,在液态铜流动过程中,表面张力的作用使氧化膜进一步破碎去除.

3 结 论

(1) 800 ℃空气中氧化过的不锈钢在 0.1 Pa 低真空加热后,表面预氧化色消失,呈现出与供应态不锈钢真空加热同等光亮度,且表面 SEM 形貌发生变化,在无腐蚀条件下能够看到晶界及晶粒的长大,同时纯铜钎料在不锈钢表面良好润湿,表明氧化膜已经在低真空下被基本去除. 而碳与 Cr_2O_3 反应热力学计算表明,在 1 000 ℃,真空度 0.1 Pa 时氧化膜确实能被碳还原.

(2) 当不锈钢表面氧化膜被弱化在应力作用下开裂时,液态铜即能渗过开裂的氧化膜润湿母材,不锈钢基体在 Ni 原子带动下向液态铜中的快速溶解对氧化膜的彻底剥离去除也起到重要作用.

参考文献:

[1] 张其枢, 堵耀庭. 不锈钢焊接 [M]. 北京: 机械工业出版社, 2003.

[2] 庄鸿寿, 罗格夏特 E. 不锈钢真空钎焊时脱氧和润湿机理 [J]. 焊接学报, 1982, 3(4): 139 - 145.
Zhuang Hongshou, Lugscheider E. The deoxidation and wetting mechanism of stainless steel in vacuum brazing [J]. Transactions of the China Welding Institution, 1982, 3(4): 139 - 145.

[3] 庄鸿寿, 罗格夏特 E. 高温钎焊 [M]. 北京: 国防工业出版社, 1989.

[4] 王立梅. 反应等离子熔敷原位合成高铬铁基复合涂层高温抗氧化性 [J]. 焊接学报, 2009, 30(1): 93 - 95.
Wang Limei. Oxidation resistance of reactive plasma cladding high chromium iron base composite coating [J]. Transactions of the China Welding Institution, 2009, 30(1): 93 - 95.

[5] 张贵锋, 张建勋, 裴 怡, 等. 相变 - 扩散钎焊工艺焊接接头缺陷分析 [J]. 焊接学报, 2004, 25(3): 93 - 96.
Zhang Guifeng, Zhang Jianxun, Pei Yi, *et al*. Analysis of transformation diffusion brazed joint [J]. Transactions of the China Welding Institution, 2004, 25(3): 93 - 96.

[6] 肖纪美. 不锈钢的金属学问题 [M]. 北京: 冶金工业出版社, 2006.

[7] 张雪峰, 方民宪, 同艳维, 等. 碳热还原法制取碳化铬、金属铬的热力学分析 [J]. 材料导报, 2010, 24(9): 108 - 113.
Zhang Xuefeng, Fang Minxian, Tong Yanwei, *et al*. Study on thermodynamic principle of preparation of Cr_3C_2 and Cr by carbon - heat reducing [J]. Materials Review, 2010, 24(9): 108 - 113.

[8] 方洪渊, 冯吉才. 材料连接过程中的界面行为 [M]. 哈尔滨: 哈尔滨工业大学出版社, 2005.

作者简介: 何 鹏, 男, 1972 年出生, 博士, 教授, 博士研究生导师. 主要从事新材料及异种材料连接基础理论与实际应用技术研究. 发表论文 105 篇. Email: hepeng@hit.edu.cn

120 mA, focus current was 763 mA and welding speed was 800 mm/min. The ratio of depth to width obviously increased with the increase of electron beam current. Tiny alteration of focus current caused significant change in the weld shape. Fine and uniform grains occurred in the weld seam, and the fracture strength, weld hardness and impact toughness of the joint reached 87%, 61% and 95.4% of those of base metal, respectively.

Key words: 7A52 aluminum alloy; electron beam welding; welding parameters; mechanical properties

Performance of dissimilar metal weld between SA335P91 and 12Cr1MoV steels in ultra(ultra) supercritical thermal power units ZHENG Kai[1,2], ZHAO Dajun[1], ZHANG Xuelian[3] (1. College of Construction Engineering, Jilin University, Changchun 130022, China; 2. Vocational and Technical College, Jilin Architectural and Civil Engineering Institute, Changchun 130118, China; 3. Guangdong Yudean Group Co., Ltd., Guangzhou 510630, China). pp 77 – 80

Abstract: Dissimilar metal welds between SA335P91 and 12Cr1MoV ferritic heat-resistant steels are widely applied in the main steam pipe and the reheater on boiler heating surface for the supercritical (SC) and ultra-supercritical (USC) thermal power units in China. The characteristics of microstructure and weldability of two steels were described, and the welding mechanism for dissimilar metal weld between two steels was investigated. Through theoretical analysis and experiments, the main factors in dissimilar metal welding that resulted in hot and cold cracks, decrease of toughness, embrittlement and type IV softening cracking tendency were determined. Corresponding technological methods and heat treatment procedures to prevent the above defects were proposed and solid joints were achieved.

Key words: supercritical; ultra-supercritical; dissimilar heat resistant steel; ferrite; welding

Microstructure and mechanical properties of thick titanium alloy joint in narrow-gap TIG welding LÜ Shixiong[1], CUI Qinglong[1], HUANG Yongxian[1], ZHENG Chuanqi[1], WANG Yang[2] (1. State Key Laboratory of Advanced Welding and Joining, Harbin Institute of Technology, Harbin 150001, China; 2. Qianjiang Motorcycle Co., Ltd., Wenling 317500, China). pp 81 – 84

Abstract: High-quality joint of thick TC4 titanium alloy plate was made by narrow-gap tungsten inert gas (TIG) welding with proper gas protection and welding parameters. Metallographic analysis of the resultant joints revealed the rules of grain growth and microstructure characteristics. The variation of the cooling speed resulted in different microstructures in the heat-affected zone (HAZ). The tensile test showed that the average tensile strength of the joints reached 90% of that of the base metal, which was attributed to the mechanism of meshing strengthening during narrow-gap TIG welding of thick titanium alloy plate.

Key words: thick titanium alloy plate; narrow-gap TIG welding; microstructure; mechanical property

Effects of surface absorption of Ge on Sn2.5Ag0.7Cu/Cu interfacial reaction and wettability YANG Tuoyu[1], MENG Gongge[2], CHEN Feng[1], XIA Xianming[1] (1. School of Mechanical Electronic and Vehicle Engineering, Anhui Science and Technology University, Anhui 233100, China; 2. School of Materials Science and Engineering, Harbin University of Science and Technology, Harbin 150040, China). pp 85 – 88

Abstract: The evolution of wetting property and interfacial morphology of Sn2.5Ag0.7Cu solder was investigated before and after adding active elements. The spreading areas of solder with different contents of Ge were measured, and the morphology of the compound was analyzed with SEM. The relationship between tension on the solid-liquid interface and the absorption amount of active elements on the same place during soldering and its effect on wetting properties were studied. The results showed that when the Ge content in solder was 0.5%, its absorption on the interface quickly raised, the forward-growing tendency of the compound was strong, and the spreading area was the largest. When the Ge content in solder was 1.0%, the absorption remained obvious but the wetting performance was weakened, and the thickness of the compound was relatively thinner. This phenomenon indicates that Ge can reduce the tension on the soldering interface within a certain range. In addition, when the absorption was relatively large, the diffusion between Cu and solder can be restrained and the growth of the compound can be hindered.

Key words: lead-free solder; active element; soldering interface; adsorption

Influence factors of dynamic recrystallization of 7050 aluminium alloy friction stir weld ZHANG Chengcong[1], CHANG Baohua[1], TAO Jun[2], ZHANG Tiancang[2] (1. Key Laboratory for Advanced Materials Processing Technology, Ministry of Education, Tsinghua University, Beijing 100084, China; 2. Research Office for Aero Engine Technology, Beijing Aeronautical Manufacturing Technology Research Institute, Beijing 100024, China). pp 89 – 92

Abstract: Friction stir welding of 7050 aluminum alloy under different rotation rates and tool traverse speeds was conducted and the influence of welding parameters on the grain size of nugget zone was investigated. To analyze the affecting mechanism of welding parameters on the grain size of nugget zone, isothermal compression experiments under different strain rates and deformation temperatures were performed and the influence of deformation parameters on the dynamic recrystallization was analyzed. Results showed that grain size in nugget zone changed slightly with the increase of the rotation rate, while it decreased with the increase of tool traverse speed. Within the range of complete dynamic recrystallization, the recrystallization grain size decreased with increase of the value of ln$Z$. The welding parameters affected the Zenner-Hollomon parameter and then determined the grain size in nugget zone.

Key words: 7050 aluminum alloy; friction stir welding; dynamic recrystallization; thermal-physical simulation

Analysis on mechanism of removing oxide film on stainless steel by heating in low vacuum HE Peng[1], ZHENG Yansong[1], LI Jun[1,2], QIAN Yiyu[1], LOU Haoyue[2], ZHANG Wenfeng[2] (1. State Key Laboratory of Advanced Welding and Joining, Harbin Institute of Technology, Harbin 150001, China; 2. Yinlun Machinery Co., Ltd., Taizhou 317200, China). pp 93 – 96

Abstract: In low vacuum condition, 0Cr18Ni9 stainless steel sheets, with one in supply state and the other pre-oxidized at 800 ℃ in air, were heated, and the steel sheet in supply state

was soaked in molten copper. It was found that the structure of oxide film changed after heating in low vacuum environment, and this film can not prevent the solution of stainless steel by the molten copper. Through investigation into the mechanism of removing oxide film on stainless steel sheet in vacuum condition and thermodynamic calculations, it was proposed that carbon could deoxygenate and weaken the oxide film. Once the molten copper met the stainless steel substrate by flowing through the cracked oxide film, the stainless steel would rapidly dissolve due to the diffusion of Ni atoms into the molten copper, and subsequently the oxide film would float on the molten copper. Finally, the oxide film would be removed under the action of surface tension in low vacuum condition.

Key words: brazing of stainless steel in low vacuum condition; mechanism of removing oxide film; carbon reductive; oxide film; solution

Optimizing of compressive stress region by local treatment technologies on Francis runner CHENG Guangfu[1], WANG Huiting[1], JI Shude[2], FANG Hongyuan[3] (1. State Key Laboratory of Hydro-power Equipment, Harbin Institute of Large Electrical Machinery, Harbin 150040, China; 2. Institute of Astronautical Technology, Shenyang Institute of Astronautical Engineering, Shenyang 110034, China; 3. State Key Laboratory of Advanced Welding and Joining, Harbin Institute of Technology, Harbin 150001, China). pp 97 – 100

Abstract: The existing of residual compressive stress increases the fatigue resistance of welding structures. The local compressive stress was realized around the fusion boundary in the Francis turbine runner by optimizing the welding process, where fracture could easily occur. And the influence of local heating and peening on the stress field in the fracture-easily-occurred region of runner was simulated and measured based on the real runner. The results indicate that the stress field in the fracture-easily-occurred region of runner can be regulated and controlled by local heating and peening processes. And the local compressive stress region was optimized. The value of residual compressive stress in the fracture-easily-occurred region of runner was further improved, and high compressive stress region was formed, especially, the compressive stress region was expanded. These processes can promote the realization of local compressive stress in the fracture-easily-occurred region of Francis runner and effectively enhance the fatigue resistance of the runner.

Key words: Francis runner; welding residual stress; local heating; peening; local compressive stress

Analysis on cooling flow field of electrode in plasma arc cutting torch CHEN Lihua[1], WEI Jingyu[2] (1. Department of Mechanical Engineering, Changzhou Institute of Mechatronic Technology, Changzhou 213002, China; 2. Hehai University Changzhou 213002, China). pp 101 – 104

Abstract: Two-dimensional numerical model for the cooling channel and electrode in plasma cutting torch was established with FLUENT commercial software, the relationship between the coolant flow field and geometry structure of the electrode was analyzed and the effects of four different electrode structures on the distribution of cooling flow field were investigated. For A-type electrode, there existed a zone where the flowing speed of the coolant was zero. For B-type electrode and C-type electrode, there was a back-flowing zone and zero-speed zone. For D-type electrode, the arc transition in the cone-shaped electrode was beneficial to cooling of the electrode. Meanwhile, the effect of inserting depth of capillary tube on the cooling flow was simulated. When the ratio of inserting depth of capillary tube to the diameter of capillary tube was larger than 0.5, there existed a zero-speed zone, however, when the ratio was around 0.2, the distribution of fluid flow field was beneficial to cooling of the electrode.

Key words: inner structure of electrode; numerical simulation; flow field

Design and realization of fully digital intelligent pulse arc welding power source DUAN Bin, ZHANG Chenghui, SUN Tongjing, ZHANG Guangxian (School of Control Science and Engineering, Shandong University, Jinan 250061, China). pp 105 – 108

Abstract: Welding power supply system with high performance is the key to meet the requirement of pulse welding technology, which can generate accurate welding arc and high welding quality. First, the system design program was proposed for fully digital pulse inverter welding power supply, including the main circuit structure and hardware circuit of the control system, based on field programmable gate array and 32-bit microcontrol unit. Second, the software design for the main control system was described using very high-speed integrated circuit hardware description language to realize the complex pulse welding technology sequence and steady arc control. Effective methods were investigated to improve the anti-interference capability and real-time performance of the system. Finally, the experiments were conducted, and the results showed that the designed fully digital intelligent pulse arc welding power source had high flexibility, robustness and reliability, which could satisfy rigorous demand of the welding arc so as to achieve satisfactory welding quality.

Key words: arc welding power source; field programmable gate array; hardware description language; anti-interference

Microstructure and mechanical properties of IC10 single crystal superalloy transient liquid phase diffusion bonding joint LANG Bo, HOU Jinbao, WU Song (Aero-Engine Technology Deptartment, Beijing Aeronautical Manufacturing Technology Research Institute, Beijing 100024, China). pp 109 – 112

Abstract: Microstructural evolution of transient liquid phase (TLP) diffusion bonding joint of IC10 single crystal superalloy was investigated with scanning electron microscopy (SEM) and energy-dispersive spectrum (EDS). The results show that the joint contained bonding zone and base material zone. The bonding zone consisted of isothermal solidification zone and rapid solidification zone. Rapid solidification zone could be eliminated by increasing welding time. The size of γ' phase in the base material reached 0.9 μm when the welding time increased from 2 h to 8 h. The mechanical properties of the joints can be effectively improved by restraining formation of grain boundary in TLP diffusion bonding joint and postweld solution treatment. The average tensile strength of the joints was 507 MPa at 1 000 ℃. The creep rupture life of the joints reached 120 h under the condition of 144 MPa stress at 1 000 ℃.

Key words: IC10 single crystal superalloy; TLP diffusion bonding; microstructure